Prediction of Chloride Penetration in Concrete and Durability Assessment Using Bayesian Optimized Long Short-Term Memory Networks

Lingjie Wu, Yufeng Xia, Fenfei Shi, Xuping Ni

Abstract—**Based on 600-day chloride penetration data from a coastal site, this study develops a deep learning model for predicting chloride transport in coastal concrete structures. The long short-term memory (LSTM) model was optimized using the Bayesian optimization algorithm (BOA). Results show that the training root mean square error (RMSE) generally decreases with increases in the number of LSTM layers, initial learning rate, and learning rate drop period, while a higher dropout rate increases RMSE. The impact of mini-batch size is irregular and negligible. The Bayesian-optimized LSTM (BO-LSTM) model outperforms the standard LSTM, convolutional neural networks (CNN), and gated recurrent unit (GRU) models in predicting chloride profiles, achieving a R^2 of 0.9743 on the validation set. The model accurately predicts chloride profiles for 600-day exposure and reliably forecasts 720-day profiles. Further analysis of influence of the age factor (m) on durability reveals that incorporating time-dependent chloride diffusion characteristics is critical for accurate assessments. Corrosion initiation times calculated using m values from measured and predicted data (62.6 and 49.2 years, respectively) align more closely with the 50-year design life than predictions ignoring time dependency. This study demonstrates the potential of deep learning for evaluating concrete durability under chloride-induced corrosion.**

Index Terms—**Concrete durability, Chloride, Long Short-Term Memory network, Bayesian optimization, corrosion initiation time**

I. Introduction

In coastal and inland saline soil environments, chloride ion penetration is a primary cause of durability degradation in concrete structures due to reinforcement corrosion [1]. Understanding the time-dependent transport mechanisms of chloride ions in concrete is critical for predicting corrosion initiation, delaying concrete cover cracking, and enhancing durability in marine environments [2–4].

Extensive experimental and theoretical research on chloride-induced concrete corrosion has been conducted over decades [1–4]. With the accumulation of experimental data, machine learning has gained prominence in this field [5–9]. However, traditional machine learning often faces a trade-off: oversimplification with basic functions or over-fitting with complex models [9]. Deep learning overcomes these limitations by leveraging multiple hidden layers to capture intricate nonlinear relationships [9, 10].

Recent advances in deep learning have expanded its applications in civil engineering [11–16], yet studies on concrete durability under chloride exposure remain limited. Wu et al. [14] compared deep learning models (LSTM, CNN, GRU, Bi-LSTM) with traditional methods (BP, SVM) for predicting time-dependent chloride transport, demonstrating superior performance of LSTM-based approaches. Hosseinzadeh et al. [15] developed a deep learning framework to predict chloride migration coefficients and compressive strength using 1,100 experimental data points, achieving >0.85 accuracy via a Python web interface. Shin et al. [16] proposed a CNN-based regression model to estimate chloride diffusion coefficients by analyzing concrete surface images.

The performance of deep learning models heavily depends on hyperparameter settings, making hyperparameter optimization (HPO) crucial for accuracy [17–21]. Xiao [20] achieved >90% accuracy in post-disaster bridge detection using Bayesian optimization (BO) for deep learning parameter tuning. Chou et al. [21] improved recognition accuracy by 1.2% for concrete beam deflection via the Jellyfish search optimization algorithm.

Despite these advances, existing research exhibits two key gaps: overreliance on CNN-based image analysis for chloride durability studies, with limited exploration of time-series regression [11–16]. HPO applications predominantly focused on traditional machine learning, neglecting deep learning models [20, 21].

Given the time-dependent and nonlinear nature of chloride penetration, deep learning-based time-series prediction offers significant potential. Furthermore, integrating model predictions with the age factor (m) — a key parameter for chloride transport characterization — can improve durability assessments.

To address these challenges, this study introduces a Bayesian optimized LSTM (BO-LSTM) framework for predicting chloride penetration profiles and assessing concrete durability. Our approach diverges fundamentally from prior works in three aspects. By integrating Bayesian optimization (BOA) with LSTM, we resolve the empirical trial-and-error dilemma in hyperparameter selection (e.g.,

Manuscript received October 21, 2024; revised March 14, 2025.

This work was supported in part by the National Natural Science Foundation of China (52008317) and the Natural Science Foundation of Zhejiang Province (LQ20E080024).

Lingjie Wu is an associate professor at the College of Civil Engineering and Architecture, Wenzhou University, Wenzhou 325035, China (e-mail: wulingjie01@wzu.edu.cn).

Yufeng Xia is a postgraduate student at the College of Civil Engineering and Architecture, Wenzhou University, Wenzhou 325035, China (e-mail: 22461544075@stu.wzu.edu.cn).

Fenfei Shi is a senior engineer at the Wenzhou Fire Rescue Detachment, Wenzhou 325000, China (e-mail: 13857771518@163.com).

Xuping Ni is an associate professor at the College of Intelligent Architecture, Zhejiang College of Security Technology, Wenzhou 325016, China. (Corresponding author, e-mail: 15066036@zjcst.edu.cn).

LSTM layer, dropout rate), achieving a 54.5% reduction in validation RMSE compared to baseline LSTM. Leveraging 600-day field data from Zhoushan coastal zone, the BO-LSTM captures nonlinear time decay of chloride diffusion coefficients (m = 0.39), enabling reliable 720-day forecasts (R^2 =0.9382) that align with Fick diffusion theory. Through Monte Carlo simulations (10 million iterations), we quantify the impact of m on corrosion initiation time, demonstrating that conventional deterministic methods underestimate service life by 67% (16.5 vs. 49.2 years). This research bridges the gap between deep learning and practical durability engineering, providing a data-driven framework for optimizing concrete mix design and maintenance strategies in marine environments.

II. Theoretical Background

A. LSTM Model

LSTM neural network is a variant of the recurrent neural network (RNN) [22]. Traditional RNNs suffer from the vanishing gradient problem, which hinders long-term memory in the network. LSTM overcomes this by using an unique architecture that effectively manages gradient flow and maintains long-term dependencies.

LSTMs achieve this through memory cells equipped with three specialized "gate" structures: the forget gate, input gate, and output gate. These gates are designed to "remember" important information and "forget" irrelevant information, enabling LSTMs to handle long sequence data [22, 23].

The forget gate f_t decides how much of the previous cell state C_{t-1} should be retained. If $f_t = 1$, the information will be retained; if $f_t = 0$, it will be forgotten. The function governing f_t is:

$$f_t = \sigma\left(W_f\left[h_{t-1}, x_t\right] + b_f\right) \tag{1}$$

where σ is the sigmoid activation function; W_f is the weight matrix for the forget gate; x_t is the current input; h_{t-1} is the previous hidden state, and b_f is the bias.

The input gate i_t selects which new information to store in the cell state. It is calculated as:

$$i_t = \sigma\left(W_i\left[h_{t-1}, x_t\right] + b_i\right) \tag{2}$$

The candidate values for updating the cell state $\tilde{C}_t$ are determined by:

$$\tilde{C}_t = \tanh\left(W_c\left[h_{t-1}, x_t\right] + b_c\right) \tag{3}$$

where W_i and b_i are the weight matrix and bias for the input gate; W_c and b_c are the weight matrix and bias for the candidate state; and tanh is the activation function used for candidate values.

The output gate o_t controls the output of the memory cell, combining the current input, previous output, and candidate state:

$$o_t = \sigma\left(W_o\left[h_{t-1}, x_t\right] + b_o\right) \tag{4}$$

The final output is:

$$h_t = o_t \tanh(C_t) \tag{5}$$

where W_o and b_o are the weight matrix and bias for the output gate.

These gates allow the LSTM model to filter out irrelevant information and manage long-term dependencies effectively, making it suitable for processing extended time series data.

B. Bayesian Optimization Algorithm

Bayesian optimization is a strategy for estimating the maximum value of an unknown function based on sampled data. It is particularly effective in solving sequential decision-making problems, helping identify the next evaluation point to achieve optimality efficiently [18, 19]. This method is particularly suitable for optimizing costly and complex functions, such as hyper-parameters in machine learning models.

For the LSTM model, hyper-parameter optimization can be framed as [18]:

$$x_{best} = \arg\min_{x \in \Omega} f\left(x\right) \tag{6}$$

where x is a multi-dimensional decision vector within the decision space Ω, defined by LSTM's preset parameters. x_{best} is the optimal set of parameters; and $f(\cdot)$ represents the optimization objective function. If the goal is maximized, the problem can be converted by considering $-f(x)$.

Bayesian optimization often employs Gaussian processes to model the objective function. For a given parameter x, the function $f(x)$ can evaluate LSTM model characteristics. To comply with Gaussian process conditions, observation noise is introduced:

$$y = f(x) + \varepsilon \tag{7}$$

where $\varepsilon \sim N(0, \sigma^2)$ represents observation error.

The observed function value y, with normal distribution noise, can ensure that evaluation of each parameter setting is independent and follows a Gaussian process. Thus, $f(x)$ can be predicted using a probabilistic model [19].

$$f\left(x\right) \sim GP\left(m\left(x\right), k\left(x, x'\right)\right) \tag{8}$$

where, GP represents Gaussian distribution; $m(x)$ is the mean value function $m\left(x\right) = E\left[f\left(x\right)\right]$; and $k(x, x')$ is the covariance function $k\left(x, x'\right) = E\left[\left(f\left(x\right) - m\left(x\right)\right)\left(f\left(x'\right) - m\left(x'\right)\right)\right]$.

The Gaussian process provides a prediction equation for the probabilistic proxy model:

$$p\left(f|X, y, x\right) = N\left(\mu\left(x\right), \sigma^2\left(x\right)\right) \tag{9}$$

where, $\mu\left(x\right) = K_*^T\left[\Sigma + \sigma^2 I\right]^{-1} y$ is the mean value of prediction results; $\sigma^2\left(x\right) = K_{**} - K_*^T\left[\Sigma + \sigma^2 I\right]^{-1} K$ is the covariance of prediction results;

$K_* = \left\{k\left(x, x_1\right), k\left(x, x_2\right), \cdots, k\left(x, x_n\right)\right\}$, $K_{**} = k\left(x, x\right)$; x is the prediction input; X represents the observation point set $\left\{x_1, x_2, \cdots, x_n\right\}$; f represents the objective function result set $\left\{f\left(x_1\right), f\left(x_2\right), \cdots, f\left(x_n\right)\right\}$; and Σ represents the covariance matrix $\Sigma_{i,j} = k\left(x_i, x_j\right)$; and y is the observation value set $\left\{y_1, y_2, \cdots, y_n\right\}$.

The acquisition function determines new sampling points by comparing expectations of their improvement over current samples. The Expected Improvement (EI) function is used [18]:

$$EI\left(x\right) = E_n\left[\max\left(0, f_n^* - f\left(x\right)\right)\right] \tag{10}$$

where f^*_n is the historical optimal value after n samples, and $I(x) \geqslant 0$

The objective is to select x to maximize the expected improvement $EI(x)$. Since the new function value is unknown, the expectation can be estimated from historical observations y, leading to:

$$EI_n(x) = \sigma(x)\varphi\left(\frac{\Delta_n(x)}{\sigma(x)}\right) + \Delta_n(x)\phi\left(\frac{\Delta_n(x)}{\sigma(x)}\right) \tag{11}$$

where $\triangle_n(x) = f^*_n - \mu(x)$; $\varphi(\bullet)$ is the cumulative distribution function; and $\varphi(\bullet)$ is the probability density function of the standard normal distribution.

The maximization of $EI(x)$ typically involves first- or second-order optimization algorithms to identify new "potential" evaluation points.

C. Prediction of Chloride Profiles Using Bayesian Optimized LSTM Model

Chloride penetration in concrete exhibits time-dependent and nonlinear behavior, making it well-suited for LSTM-based time series prediction. The proposed framework integrates a Bayesian-optimized LSTM model composed of four components: input layer, hidden layer, Bayesian optimization module, and output layer.

Input layer: this layer preprocesses raw data to meet network requirements, including: splitting data into training and validation sets; normalizing features to prevent gradient divergence during training.

Hidden layer: the core component consists of LSTM cells forming a recurrent neural network. By default, an LSTM layer with 128 units is employed and trained via the Adam optimizer. Increasing the number of units may improve accuracy but risks overfitting, necessitating Bayesian optimization for balance.

Bayesian optimization module: this module optimizes five hyperparameters: LSTM layer, dropout rate, initial learning rate, learning rate drop period, and mini-batch size. The objective is to minimize training root mean square error (RMSE), where Bayesian optimization iteratively selects hyperparameter combinations to maximize model efficiency and generalizability.

Output layer: model performance is evaluated using four metrics: coefficient of determination (R^2), RMSE, mean absolute error (MAE), and mean absolute percentage error (MAPE).

These metrics are calculated as follows [22, 23]:

$$\mathrm{R}^2 = 1 - \frac{\sum_{i=0}^{n}\left(y_i - y_i^{'}\right)^2}{\sum_{i=0}^{n}\left(y_i - \bar{y}\right)^2} \tag{12}$$

$$\mathrm{MAE} = \frac{1}{n}\sum_{i=1}^{n}\left|y_i - y_i^{'}\right| \tag{13}$$

$$\mathrm{MAPE} = \frac{1}{n}\sum_{i=1}^{n}\left|\frac{y_i - y_i^{'}}{y_i}\right| \tag{14}$$

$$RMSE = \sqrt{\frac{1}{n}\sum_{i=1}^{n}\left(y_i - y_i^{'}\right)^2} \tag{15}$$

where, n is the number of samples; y_i' is the predicted value of neural network; and y_i is the measured value.

This approach ensures that the LSTM model accurately predicts chloride profiles while effectively handling both the temporal and nonlinear nature of the data.

III. Results and Discussion

A. Overview of Chloride Corrosion Testing and Data Collection

The chloride corrosion test was conducted in the tidal zone of a coastal wharf in Dinghai New City, Zhoushan, China. The location has an average annual temperature of 20°C and a humidity of 79%. The site was submerged in seawater for approximately 4.5 hours daily. Analysis of on-site water samples revealed a free chloride ion content of about 1.3% [14].

Cylindrical concrete samples (Ø100 mm × 50 mm) were prepared using P•O32.5 R cement with a water-cement ratio of 0.45 and six samples per group. These samples were exposed to corrosion for periods of 120, 240, 360, 480, and 600 days. After each exposure period, samples were ground in 2 mm increments from the surface inward to measure free chloride ion content. The averaged results are shown in Fig. 1.

The experiment yielded a total of 300 data points. The first 240 data points corresponded to 120, 240, 360, and 480 days of exposure. Of these, 90% were allocated to training the LSTM model, and the remaining 10% were used for validation. The trained model was then used to predict the chloride concentration profiles at 600 days, which were compared with actual measurements to validate the model's effectiveness.

Given the consistent water-cement ratio, fixed 120-day sampling interval, and uniform sample size, chloride concentration was the sole input and output variable in this time series prediction experiment.

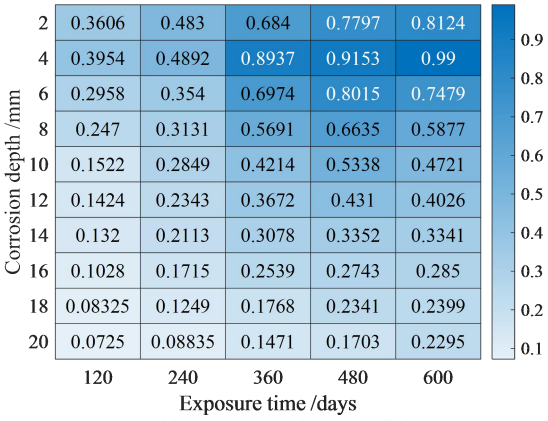

Fig. 1 Chloride content data from field test

B. Hyperparameter Optimization

1) Bayesian Hyperparameter Optimization

To achieve accurate chloride concentration profile predictions, this study employs BO for intelligent parameter tuning. The number of LSTM layers was set between 32 and 512, adjusted in increments of 32 units based on the training set size. The initial learning rate ranged from 0.0005 to 0.01, modified in increments of 0.0005 units, while the learning rate drop period spanned from 10 to 300, adjusted in increments of 10 units. To prevent over-fitting in large neural networks, a dropout layer was incorporated, with the dropout probability ranging from 0.05 to 0.5 in increments of 0.05.

Research indicates that the convergence rate and accuracy of LSTM are sensitive to the mini-batch size setting [19], requiring its optimization within the range of 32 to 320, adjusted in increments of 32 units.

Applying Bayesian global optimization to these five parameters resulted in 960,000 possible combinations (16 × 20 × 30 × 10 × 10), which significantly impacted computational efficiency. Therefore, we first analyzed the influence of each parameter on the model's training RMSE to reduce the number of parameters subject to global optimization. This preliminary analysis enabled identification of optimal parameter values prior to Bayesian global optimization. Fig. 2 illustrates the impact of these five parameters on training RMSE after 30 BO iterations.

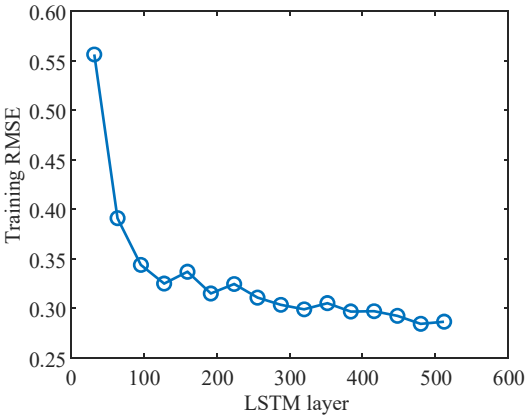

(a)

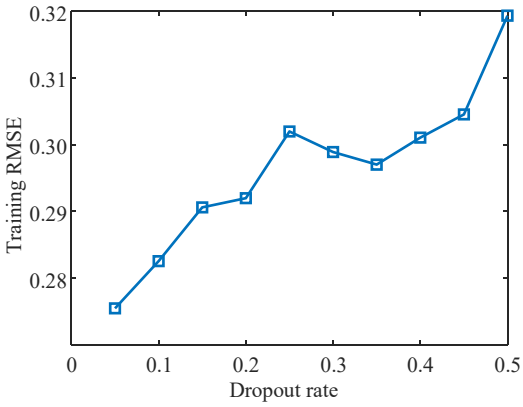

(b)

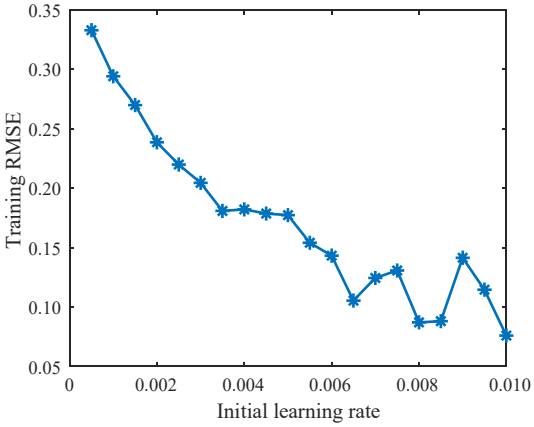

(c)

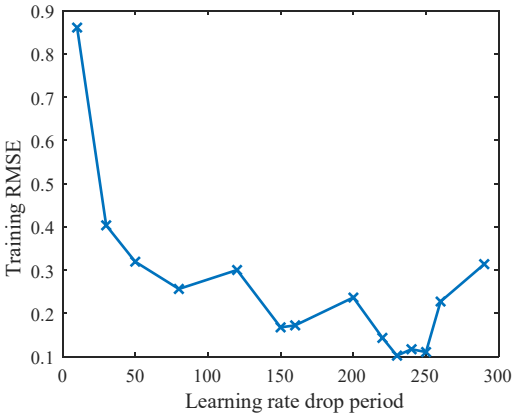

(d)

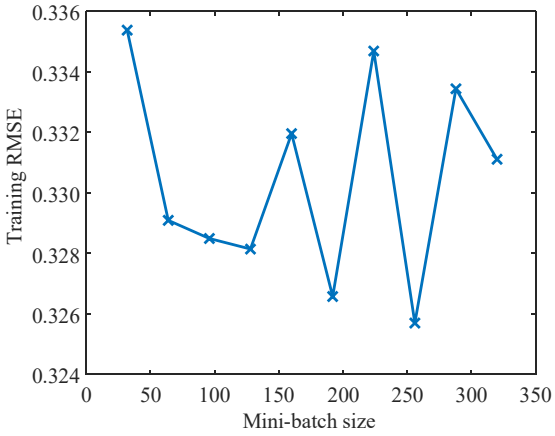

(e)

Fig.2 Influence of model parameters on training RMSE

Fig. 2 demonstrates that increasing the number of LSTM layers, initial learning rate, and learning rate drop period generally reduces training RMSE, whereas a higher dropout rate increases it. The influence of mini-batch size on training RMSE is minimal and irregular, varying from 0.3257 to 0.3354 as it ranges from 32 to 320. Consequently, the effect of mini-batch size can be ignored during hyperparameter optimization, and a default value of 128 is used. When the number of LSTM layers is small, increasing them effectively reduces training RMSE. Beyond 128 layers, the reduction in RMSE diminishes. Previous studies have shown that excessively large LSTM layers may cause over-fitting [18, 19], leading to the selection of 500 layers for this study. For the learning rate drop period, values above 80 results in RMSE fluctuations; thus, with 500 LSTM layers, a drop period of 100 is appropriate. The dropout rate and initial learning rate were set to 0.05 and 0.01, respectively, based on Figs. 3(b) and (c). These adjustments reduced Bayesian optimization iterations from 960,000 to 150. However, this analysis focuses on single-parameter optimization, and interactions between parameters in global optimization may yield different effects. Fig. 3 presents the impact on training RMSE after 250 BO iterations with global optimization of dropout probability and initial learning rate.

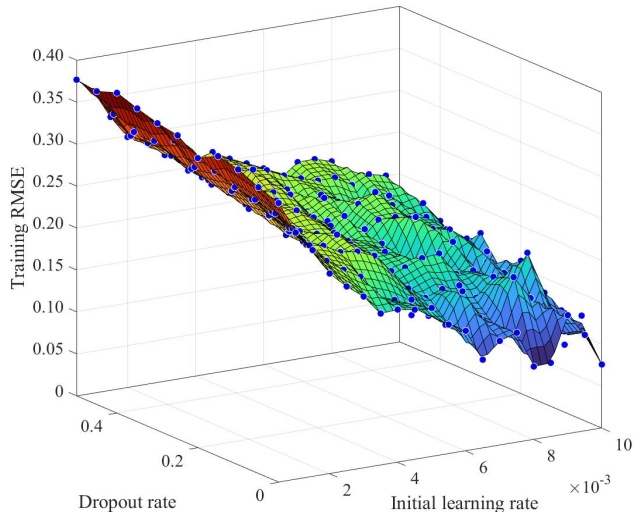

(a)

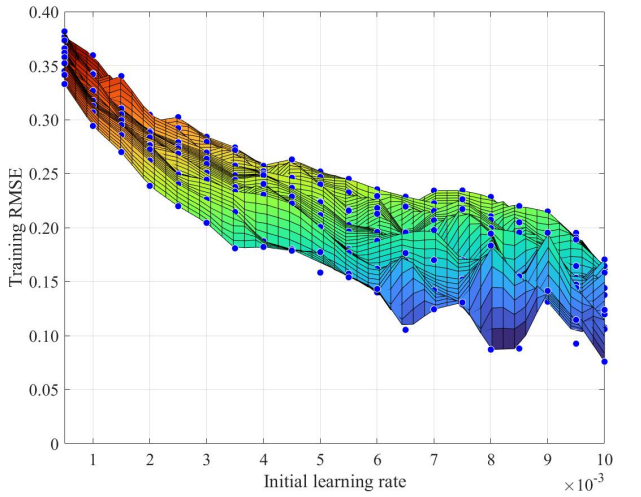

(b)

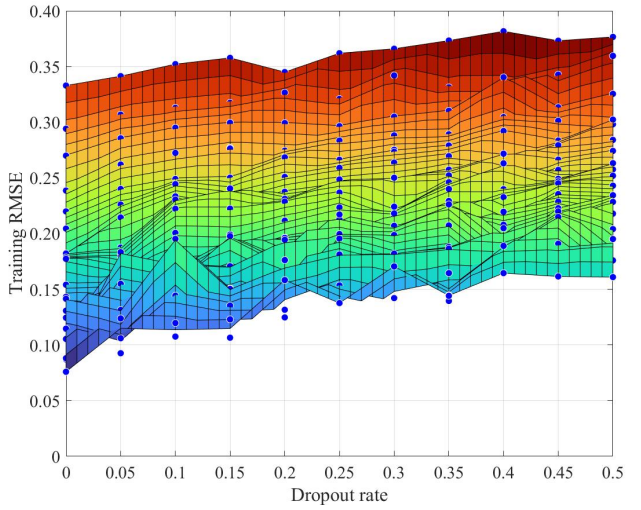

(c)

Fig.3 Influence of dropout layer and initial learning rate on Training RMSE

Analyses of Figs. 2 and 3 reveal that the effects of dropout probability and initial learning rate on training RMSE align with results from individual optimizations even during global optimization. Specifically, a higher initial learning rate and a lower dropout probability contribute to reduced training RMSE. This validates that the proposed simplified Bayesian single-parameter optimization method is reasonable and effective, significantly improving optimization efficiency.

The parameter settings for the BO-LSTM model are detailed in Table I. To assess the predictive accuracy of the BO-LSTM model, a comparative analysis with the standard LSTM model was conducted, with both models' parameters provided in Table I.

TABLE I
LSTM MODEL PARAMETERS

	LSTM layer	Dropout layer	Initial learning rate	Mini-batch size
BO-LSTM	500	0.05	0.01	128
LSTM	128	0.2	0.001	128
GRU	128	0.2	0.001	128
CNN	(3,64)	0.2	0.001	128

After 500 iterations, Table II presents the evaluation metrics for the LSTM and BO-LSTM models using validation data.

TABLE II
EVALUATION INDICATOR

	R^2	RMSE	MAE	MAPE
BO-LSTM	0.9743	0.0402	0.0309	5.8776%
LSTM	0.9372	0.0668	0.0536	13.6668%
GRU	0.9684	0.0477	0.0358	7.3283%
CNN	-0.3522	0.3104	0.2539	60.6480%

Table II compares the performance of four predictive models: LSTM, GRU, CNN, and BO-LSTM. While the LSTM model demonstrates strong performance, it is slightly inferior to the BO-LSTM model. Specifically, although the LSTM achieves a high R^2 value, its RMSE and MAE are higher than those of BO-LSTM, and its MAPE is significantly larger. This indicates that the LSTM model generates larger prediction errors at specific points. Although LSTM is effective in capturing long-term dependencies, its complex architecture with more parameters may result in over-fitting or under-fitting, particularly with limited data or insufficient feature diversity [9, 10].

The GRU model demonstrates performance comparable to BO-LSTM. This phenomenon can be explained by GRU's simplified architecture: unlike LSTM's three-gate mechanism (forget gate, input gate, and output gate), GRU manages information flow solely through a reset gate and an update gate. This structural difference reduces GRU's parameter count by approximately 33%, granting it significant advantages in scenarios with limited data volume (300 samples) or low feature complexity [14]. However, GRU's limitations become evident in long-term dependency modeling: the absence of an independent "forget gate" may impair its ability to precisely capture complex nonlinear temporal patterns, such as the exponential decay of chloride diffusion coefficients over time. Consequently, GRU is better suited for short-term predictions or feature-simple tasks, while LSTM excels in handling complex temporal sequences.

In contrast, the CNN model performs poorly, as evidenced by a negative R^2 value. This suggests that the CNN's predictions are less accurate than a simple mean-based baseline. The high RMSE and MAE, combined with an exceptionally high MAPE, indicate substantial errors across most observations. Although CNNs are proficient at

extracting local spatial features and can identify local temporal patterns through convolutional kernels, they fail to capture long-term dependencies in datasets with complex temporal structures [14–16].

Overall, the BO-LSTM model outperforms all other models across all metrics. Its R^2 value approaches 1, indicating excellent data fit. Additionally, its lower RMSE and MAE reflect minimal prediction errors, while a moderate MAPE suggests consistent relative accuracy. The integration of Bayesian optimization enables selection of optimal hyperparameters, ensuring the model achieves the best possible configuration. This optimization significantly improves predictive performance.

2) Sensitivity Analysis

While methods such as SHapley Additive exPlanations and Local Interpretative Model-agnostic Explanations are widely used to enhance the interpret-ability of deep learning models by analyzing input data [8], this study focuses exclusively on exposure time variations and thus omits interpret-ability analysis. To investigate the effects of model parameters on predictions, a sensitivity analysis was conducted on the number of LSTM layers, dropout probability, and initial learning rate. Each parameter was reduced by 50%, and changes in evaluation metrics were quantified (detailed in Table I). These changes were normalized and visualized in Fig. 4.

For the BO-LSTM model, optimization preferred a higher number of LSTM layers. Reducing the layer count from 500 to 250 significantly degraded prediction accuracy. This sensitivity arises from the hierarchical modeling capability of deep LSTM networks, which capture both long-term dependencies (e.g., the exponential decay of chloride diffusion coefficient) and local nonlinearities (e.g., abrupt changes in surface chloride concentration) through chained gated units. Bayesian optimization mitigates over-fitting risks by dynamically adjusting the dropout probability (0.05) and initial learning rate (0.01), ensuring the model adheres to physical laws while suppressing noise. This mechanism aligns with the time-dependent diffusion framework of Fick's law, validating the physical consistency of deep LSTM in durability assessment. Furthermore, Fig. 4 emphasizes the dominance of LSTM layer count in prediction accuracy, necessitating joint optimization of dropout probability and initial learning rate with layer count rather than isolated adjustments.

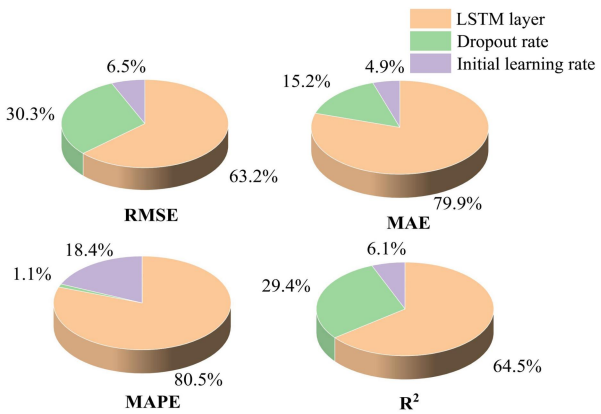

Fig. 4 Sensitivity analysis of model input parameter

3) Impact of Data Preprocessing

This study revealed that data preprocessing methods significantly affect model prediction accuracy. Previous research demonstrates that effective preprocessing enhances the performance and robustness of LSTM models [15, 19]. In the initial stage, the measured chloride ion concentration was directly employed as both the input and the output, and the evaluation metrics are presented in Table II. In an alternative approach, corrosion depth and exposure time were used as the inputs, while chloride ion concentration is used as the output. Results for the latter approach (using the same model parameters from Table I) are shown in Table III.

A comparison of Tables II and III shows that using multiple input parameters led to a decline in all four evaluation metrics. This decline may stem from the complex nonlinear relationships between the inputs and output, which cannot by fully captured by the LSTM model. Specifically, chloride ion concentration non-linearly decreases with increasing corrosion depth and increases with extended exposure time [2–4]. When both parameters are used as the inputs, the combined nonlinear relationship becomes more intricate, further challenging the LSTM's modeling capability and resulting in reduced performance.

TABLE III
EVALUATION INDICATOR

Model	R^2	RMSE	MAE	MAPE
BO-LSTM-Data	0.9041	0.0837	0.0617	11.9598%
LSTM-Data	0.8825	0.0922	0.0746	15.8448%
BO-CNN-LSTM-Data	0.9331	0.0693	0.0476	10.1322%
CNN-LSTM-Data	0.9100	0.0806	0.0581	11.1340%

To improve accuracy, a hybrid CNN-LSTM model was implemented, where the CNN extracts local spatial features and the LSTM captures temporal dependencies [23]. As shown in Table III, this hybrid model outperforms the standalone LSTM across all evaluation metrics. However, compared to the results in Table II (using direct chloride concentration as input-output), its accuracy remains lower. This suggests that using measured chloride concentration directly can capture time-series trends in a more effective way. The strong input-output correlation simplifies the LSTM's learning process, leading to higher prediction accuracy.

C. Prediction of Chloride Transport in Concrete

Using the trained BO-LSTM model, this study predicted chloride concentration profiles for concrete exposed to chloride environments over 600 days. The predicted values closely match the measured data (correlation coefficient = 0.9811), with evaluation metrics RMSE = 0.0646, MAE = 0.0476, MAPE = 9.24%, and R^2 = 0.9382 (Fig. 5). These results demonstrate that the BO-LSTM model achieves reliable short-term predictions of chloride penetration in concrete.

Using 300 field test samples for training and validation, the BO-LSTM model was extended to predict chloride profiles for 720 days of exposure (Fig. 6). The predicted profiles show a gradual increase in chloride concentration over time, consistent with the accumulation mechanism of chloride ions in concrete.

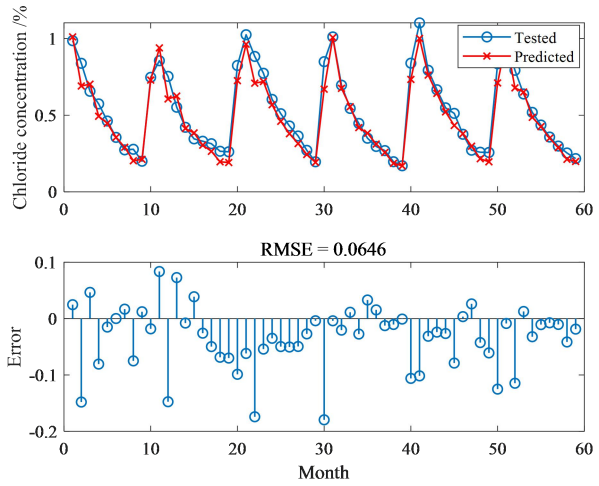

Fig. 5 Chloride profiles predicted by BO-LSTM

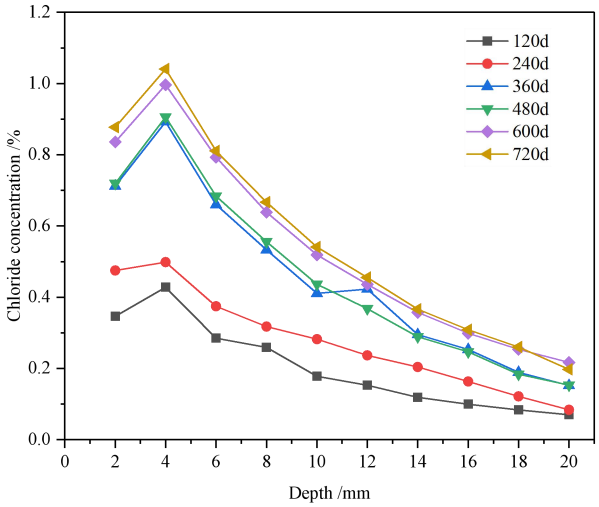

Fig. 6 Chloride profiles of concrete from 120d to 720d

When the experimental data was fitted to Fick's second law, the apparent chloride diffusion coefficients were determined to be 1.805, 1.578, 1.24, 1.064, 0.8196, and 0.6511 × 10^{-12} m^2/s. These calculated values lie within the typical range of 10^{-11} to 10^{-14} m^2/s as reported in previous research [24], which validates their reliability. The decline in the diffusion coefficient over time, as observed, can be attributed to the pore - filling effects resulting from the continuous cement hydration process [25–27]. The time-dependent chloride diffusion coefficient is modeled by Eq. (16) [28]:

$$D(t) = D_0 \left(\frac{t_0}{t} \right)^m \tag{16}$$

where $D(t)$ and D_0 are the chloride diffusion coefficients at times t and t_0, respectively.

Using the 600 - day data, the value of m was fitted to be 0.48. When the 720 - day predictions were taken into account, m was adjusted to 0.39. This adjusted value is in line with the literature values ranging from 0.2 to 0.55 [27 – 31]. The decrease and subsequent stabilization of m over time are consistent with the well - established trends reported in the relevant literature [28, 29].

D. Durability Implications of m

To assess the impact of m on concrete durability, corrosion initiation time was evaluated using Fick's second law, considering concrete cover depth d, surface chloride concentration C_s, and critical chloride concentration C_{cr}. While Eq. (17) provides a basic estimation, it neglects time-dependent diffusion characteristics. Substituting Eq. (16) into Fick's law yields Eq. (18), but literature recommends Eq. (19) for improved accuracy [25]:

$$t_1 = \frac{d^2}{4D_0} \cdot \left(erf^{-1}\left(\frac{C_s - C_{cr}}{C_s} \right) \right)^{-2} \tag{17}$$

$$t_2 = \left[\frac{d^2}{4D_0 \cdot t_0^m} \cdot \left(erf^{-1}\left(\frac{C_s - C_{cr}}{C_s} \right) \right)^{-2} \right]^{\frac{1}{1-m}} \tag{18}$$

$$t_3 = \left[\frac{(1-m)d^2}{4D_0 \cdot t_0^m} \cdot \left(erf^{-1}\left(\frac{C_s - C_{cr}}{C_s} \right) \right)^{-2} \right]^{\frac{1}{1-m}} \tag{19}$$

Table IV lists the parameters derived from field data and specifications [32]. Substituting these into Eqs. (17)–(19), corrosion initiation times were calculated (Fig. 7). Eq. (17) predicts an unrealistic 40.73 years, while Eq. (18) overestimates due to its use of an instantaneous diffusion coefficient. Even Eq. (19) overestimates, highlighting the limitations of deterministic approaches that ignore parameter variability [31–33].

TABLE IV
CALCULATION PARAMETERS FOR CORROSION INITIATION TIME

	m	C_s	d	D_0	t_0	c_{ar}
Tested	0.48	1.45%	50	0.8196×10^{-12}	600d	0.4%
BO-LSTM	0.39	1.45%	50	0.8196×10^{-12}	600d	0.4%

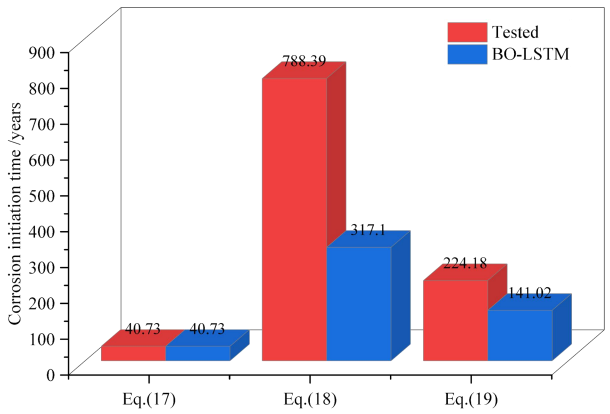

Fig. 7 Corrosion initiation time /years

To address this, a probabilistic approach was adopted, assuming normally distributed parameters (coefficient of variation = 0.1). A Monte Carlo simulation with 10^7 iterations (Fig. 8) shows that corrosion initiation time reaches 62.6 years for m = 0.48 and 49.2 years for m = 0.39, closely matching the 50-year design lifespan. Without time-dependent considerations, the initiation time is only 16.5 years, underscoring the critical role of m.

In conclusion, incorporating time-dependent chloride diffusion characteristics is essential for durability assessment. The BO-LSTM model enables reliable adjustments to durability predictions, providing a robust tool for coastal concrete structures.

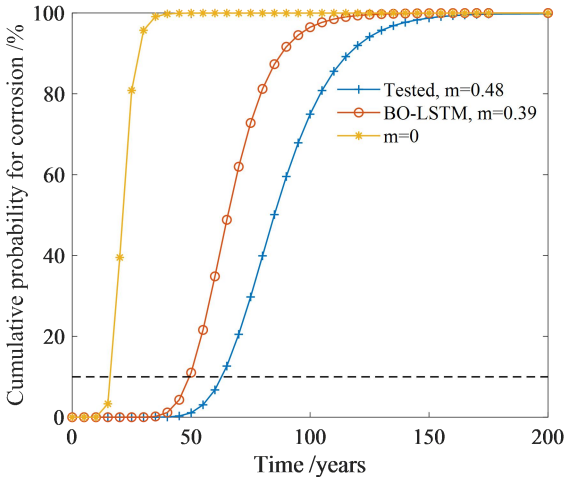

Fig.8 Cumulative probability for corrosion

IV. Conclusion

This study developed a BO-LSTM model to predict chloride transport in coastal concrete structures, yielding the following key findings:

1) Bayesian optimization effectively enhanced the prediction accuracy through the precise fine - tuning of crucial hyperparameters. During the process, as the number of LSTM layers, the initial learning rate, and the learning rate drop periods increased, the root mean square error (RMSE) of the training decreased. In contrast, an increase in the dropout rate led to an elevation in the RMSE.

2) The BO-LSTM model outperformed standalone LSTM, GRU, and CNN models in chloride profile prediction. For the validation set, the BO-LSTM model achieved an R^2 of 0.9743, RMSE of 0.0402, MAE of 0.0309, and MAPE of 5.88%, demonstrating high accuracy and reliability.

3) The model accurately predicted 600-day chloride profiles, showing a correlation coefficient of 0.9811 between predictions and measurements. For 720-day exposure, the predicted gradual chloride accumulation aligns with known concrete corrosion mechanisms.

4) The age factor derived from measured (m = 0.48) and predicted (m = 0.39) data significantly impacts corrosion initiation time. By employing these values of m, the calculated corrosion initiation times, which are 62.6 years and 49.2 years respectively, are in close agreement with the 50 - year design lifespan. This stands in contrast to the predictions made when the time-dependent diffusion characteristics are ignored.

These findings highlight the importance of integrating Bayesian optimization and time-dependent diffusion characteristics in durability assessments, providing a robust framework for evaluating concrete structures in chloride-rich environments.

References

[1] J. Z. Zhang, J. Zhao, Y. R. Zhang, Y. H. Gao, and Y. Y. Zheng, "Instantaneous chloride diffusion coefficient and its time dependency of concrete exposed to a marine tidal environment," *Construction and Building Materials*, vol. 167, pp. 225-234, 2018.

[2] D. S. Chen, W. H. Guo, B. A. Wu, and J. Shi, "Service life prediction and time-variant reliability of reinforced concrete structures in harsh marine environment considering multiple factors: A case study for Qingdao Bay Bridge," *Engineering Failure Analysis*, vol. 154, 107671, 2023.

[3] Y. Zhang, X. Y. Zhou, J. Zhao, H. X. Zhuang, Y. H. Gao, and Y.R. Zhang, "Time dependency and similarity of decay process of chloride diffusion in concrete under simulated marine tidal environment," *Construction and Building Materials*, vol. 205, pp. 332-343, 2019.

[4] L. J. Wu, W. Li, and X.N. Yu, "Time-dependent chloride penetration in concrete in marine environments," *Construction and Building Materials*, vol. 152, pp. 406-413, 2017.

[5] W. Z. Taffese, and L. Espinosa-Leal, "Prediction of chloride resistance level of concrete using machine learning for durability and service life assessment of building structures," *Journal of Building Engineering*, vol. 60, 2022.

[6] V. Q. Tran, "Machine learning approach for investigating chloride diffusion coefficient of concrete containing supplementary cementitious materials," *Construction and Building Materials*, vol. 328, 2022.

[7] R. Cai, T. H. Han, W. Y. Liao, J. Huang, D. W. Li, A. Kumar, and H. Y. Ma, "Prediction of surface chloride concentration of marine concrete using ensemble machine learning," *Cement and Concrete Research*, vol. 136, 2020.

[8] W. Z. Taffese, and L. Espinosa-Leal, "Unveiling non-steady chloride migration insights through explainable machine learning," *Journal of Building Engineering*, vol. 82, 2024.

[9] S. Q. Wang, P. Xia, K. Y. Chen, F. Y. Gong, H. L. Wang, Q. H. Wang, Y. X. Zhao, and W. L. Jin. "Prediction and Optimization Model of Sustainable Concrete Properties Using Machine Learning, Deep Learning and Swarm Intelligence: A Review," *Journal of Building Engineering* vol. 80, 2023.

[10] B. B. Guo, J. Chu, Z. D. Zhang, Y. Wang, and D. T. Niu. "Effect of External Loads on Chloride Ingress into Concrete: A State-of-the-Art Review," *Construction and Building Materials* vol. 450, 2024.

[11] F. M. Deng, Y. G. He, S. X. Zhou, Y. Yu, H. G. Cheng and X. Wu, "Compressive strength prediction of recycled concrete based on deep learning," *Construction and Building Materials*, vol. 175, pp. 562-569, 2018.

[12] S. X. Zhou, W. Sheng, Z. P. Wang, W. Yao, H. W. Huang, Y. Q. Wei, and R. G. Li, "Quick image analysis of concrete pore structure based on deep learning," *Construction and Building Materials*, vol. 208, pp. 144-157, 2019.

[13] Y. Song, Z. L. Huang, C. Y. Shen, H. Shi and D. A. Lange, "Deep learning-based automated image segmentation for concrete petrographic analysis," *Cement and Concrete Research*, vol. 135, 2020.

[14] L. J. Wu, W. Q. Wang, and C. C. Jiang. "Deep Learning-Based Prediction for Time-Dependent Chloride Penetration in Concrete Exposed to Coastal Environment," *Heliyon*, vol. 9, no. 6, 2023.

[15] M. Hosseinzadeh, H. Samadvand, A. Hosseinzadeh, S. S. Mousavi, and M. Dehestani. "Concrete Strength and Durability Prediction through Deep Learning and Artificial Neural Networks.", *Frontiers of Structural and Civil Engineering*, vol. 18, no. 10, pp. 1540-1555, 2024.

[16] H. K. Shin, H. Kim, and S. H. Lee. "Convolutional Neural Network-Based Regression for Predicting the Chloride Ion Diffusion Coefficient of Concrete," *CMC-Computers Materials & Continua*, vol. 70, no. 3, pp. 5059-5071, 2022.

[17] F. F. Abdelkader, H. Tarik, E. H. Ibtissam, and M. Tawfik, "Particle Swarm Algorithm Setting using Deep Reinforcement Learning in the Artificial Neural Network Optimization Learning Process," *IAENG International Journal of Computer Science*, vol. 51, no. 8, pp. 1195-1208, 2024.

[18] D. Soydaner, "A comparison of optimization algorithms for deep learning," *International Journal of Pattern Recognition and Artificial Intelligence*, vol. 34, no. 13, 2020.

[19] R. Y. Sun, "Optimization for deep learning: An overview," *Journal of the Operations Research Society of China*, vol. 8, no. 2, pp. 249-294, 2020.

[20] X. Liang, "Image-based post-disaster inspection of reinforced concrete bridge systems using deep learning with Bayesian optimization," *Computer-Aided Civil and Infrastructure Engineering*, vol. 34, no. 5, pp. 415-430, 2019.

[21] J. S. Chou, M. A. Karundeng, D. N. Truong and M. Y. Cheng, "Identifying deflections of reinforced concrete beams under seismic loads by bio-inspired optimization of deep residual learning," *Structural Control and Health Monitoring*, vol. 29, no. 4, 2022.

[22] Z. Y. Xu, J. Zhang, J. Y. Wang and Z. M. Xu, "Prediction research of financial time series based on deep learning," *Soft Computing*, vol. 24, no. 11, pp. 8295-8312, 2020.

[23] T. Le, M. T. Vo, B. Vo, E. Hwang, S. Rho and S. W. Baik, "Improving electric energy consumption prediction using CNN and Bi-LSTM," *Applied Sciences*, vol. 9, no. 20, 2019.

[24] G. de Vera, M. A. Climent, E. Viqueira, C. Antón and M. P. López, "Chloride penetration prediction in concrete through an empirical

model based on constant flux diffusion," *Journal of Materials in Civil Engineering*, vol. 27, no. 8, 2015.
[25] S. W. Pack, M. S. Jung, H. W. Song, S. H. Kim and K. Y. Ann, "Prediction of time-dependent chloride transport in concrete structures exposed to a marine environment," *Cement and Concrete Research*, vol. 40, no. 2, pp. 302-312, 2010.
[26] Y. M. Sun, M. T. Liang and T. P. Chang, "Time/depth dependent diffusion and chemical reaction model of chloride transportation in concrete," *Applied Mathematical Modelling*, vol. 36, no. 3, pp. 1114-1122, 2012.
[27] Q. X. Xiong, Q. F. Liu, X. J. Zhang and C. Chen, "Chloride diffusion prediction in concrete through mathematical models based on time-dependent diffusion coefficient and surface chloride concentration," *Journal of Materials in Civil Engineering*, vol. 34, no. 11, 2022.
[28] L. J. Wu, X. Gao and Y. F. Xia, "Randomness and time-varying characteristics of chloride ion transport in existing harbor concrete structures," *Construction and Building Materials,* vol. 412, 2024.
[29] K. F. Li, D. D. Zhang, Q. W. Li and Z. H. Fan, "Durability for concrete structures in marine environments of HZM project: Design, assessment and beyond," *Cement and Concrete Research*, vol. 115, pp. 545-558, 2019.
[30] U. M. Angst, "Predicting the time to corrosion initiation in reinforced concrete structures exposed to chlorides," *Cement and Concrete Research*, vol. 115, pp. 559-567, 2019.
[31] P. F. Marques, A. Costa and F. Lanata, "Service life of RC structures: chloride induced corrosion: prescriptive versus performance-based methodologies," *Materials and Structures*, vol. 45, no. 1-2, pp. 277-296, 2012.
[32] GB/T50476-2019, "Standard for design of concrete structure durability" [S]. Beijing: China Architecture & Building Press, 2019. (in Chinese)
[33] J. L. Wang, L. F. Yang, J. H. Huang and B. Yu, "Service life prediction model for marine concrete structures considering structural shape and time-dependent behaviour," *Ocean Engineering*, vol. 285, Part 1, 115276, 2023.
[34] Q. D. Nguyen and A. Castel, "Long-term durability of underground reinforced concrete pipes in natural chloride and carbonation environments," *Construction and Building Materials*, vol. 394, 132230, 2023.